Inorganic frameworks based on bimetallic nanoparticles encapsulated in hollow MnO$_2$ structures

Gema Cabello [a,b,*,1], Rogério A. Davoglio [b,*,1]

[a] School of Medicine, Medical Sciences and Nutrition, University of Aberdeen, Foresterhill, Aberdeen AB25 2ZD, United Kingdom
[b] Department of Chemistry, Universidade Federal de São Carlos, 13565-905 São Carlos, SP, Brazil

ABSTRACT

A novel microwave-assisted hydrothermal route has been demonstrated to allow the synthesis of hollow MnO$_2$ particles with dandelion-like structure. The as-prepared particles show the ability to enclose PtAu bimetallic nanoparticles which good electrocatalytic activity toward the oxidation of glycerol and the reduction of oxygen in alkaline media, in addition to high stability, what we attribute to the MnO$_2$ cage, which is responsible for the confinement of reaction intermediates impeding their diffusion to the bulk electrolyte. Considering the inherent properties of MnO$_2$, such as low acute toxicity to living organisms, biocompatibility, stability in neutral and alkaline media and the ability to enclose other possible different materials, including functionalized nanoparticles, we suggest a broad field of potential application for these structures, such as drug delivery and bioimaging, catalysis, (bio)sensing, etc.

© 2017 Elsevier B.V. All rights reserved.

1. Introduction

The development of nanostructured architectures has attracted considerable efforts in recent years paying great attention to control of structural and morphological properties. In addition, the increasing demand for novel sustainable materials, especially for applications where noble metals have been predominant, has led to new materials being developed and tested. Among different materials tested, scientific community has paid much attention to manganese dioxide because of its abundance and, therefore, low cost, high biocompatibility and easy tunable structural properties. MnO$_2$ exists in many polymorphic and structural forms, which may be attractive from the point of view that it provides a broad alternative of materials with a single phase. In addition, manganese oxide shows excellent electrochemical performance for practical applications to energy storage systems (such as electrochemical supercapacitors (ES)). Further, several attempts have been carried out to find other different applications to MnO$_2$, such as non-enzymatic amperometric sensors and biosensors for glucose and lactate detection; to immobilize proteins; for catalytic applications (as decomposition of H$_2$O$_2$), etc [1].

In addition, crystal size, structure and phase depend on the synthetic route and can be easily modified, leading to distinctive characteristics for potential improved applications. As some examples, α-MnO$_2$ nanowires have shown enhanced capacity in lithium–air batteries [2]; β-MnO$_2$ clusters have been applied as catalysts for water oxidation [3]; porous γ-MnO$_2$ has been use for aqueous alkaline cathodes; and ε-MnO$_2$ has been proved to be an efficient catalyst for the oxygen reduction reaction (ORR) [4].

In order to achieve the desired morphological properties of MnO$_2$, several synthesis methods have been proposed based on conventional routes, such as electrochemical, precipitation and sol-gel [5–9], and others involving unconventional energy sources, as sonochemical, hydrothermal and microwave [10–14]. Microwave (MW) energy has been applied for years in organic synthesis [17,18], and its use for other applications has been progressively extended in recent years to fields as different as telecommunications, diagnostics, imaging and treatment applications, security, etc. [19]. Among all, the application of MW to new materials design has attracted the attention of chemists and has emerged as a promising alternative route of synthesis. The mechanisms involving MW interaction with matter remain not well understood and, further, there is still much controversial about the existence of specific microwave effects or non-thermal effects involving changes in the magnitude of the entropy attributed to increased molecular motion [20]. Independently of the mechanisms, microwave dielectric heating provides volumetric heating and higher heating rates when at least one component couples strongly with MW radiation

* Corresponding author.
E-mail addresses: gema.cabellocarramolino@abdn.ac.uk (G. Cabello), rogeriodavoglio@gmail.com (R.A. Davoglio).
[1] These authors contributed equally to this work.

[21]. In addition, selective heating may be achieved arising from selective interactions of the components with MWs.

Synthesis routes involving liquid–liquid heterogeneous systems (organic-aqueous two-phase media) under MW irradiation have been previously reported to improve the selectivity by lowering water activity [22]. Non-polar organic solvents are almost transparent to MW radiation and can be used as coolants for removing excess heat from a microwave cavity. However, it has been shown that the mixture of a polar solvent and a non-polar solvent may lead to high heating rates for the entire mixture [21]. The versatility of microwave-assisted routes for the synthesis of inorganic materials has been widely demonstrated [23], including hollow nanoparticles [24–27]. Hollow architectures are attractive because of their high surface area, low density and the ability to enclose diverse materials with potential applications in gas adsorption, drug delivery, catalysis, sensing, etc. [28]. By serving as host cages for diverse functional species, inorganic frameworks containing small nanoparticles may help to prevent particle leaking and functionalized species from premature degradation, working as nanoscale reactors [29] which control solubility and diffusivity of species to and from the framework.

In general, we assume that the coating or encapsulation of nanoparticles is still an open research field with wide possibilities to a large variety of new designs and strategies.

In this work, we investigate the three-phase synthesis of MnO_2 hollow nanocages under microwave irradiation (in the absence of a template and/or surfactant), in addition to the encapsulation of PtAu bimetallic nanoparticles. The system has been investigated for several applications, including the reduction of oxygen and the oxidation of glycerol. It is suggested that MnO_2 hollow frameworks may serve as a basis for designing novel hybrids, suited to hold different materials such as magnetic particles, biological nanostructured materials, etc. for very diverse applications.

2. Experimental

2.1. Chemicals and instrumentation

All reagents were analytical grade, in the purest commercially available grade. All solutions were prepared using Milli-Q water (18.2 MΩ cm, Millipore). MnO_2 and NPs synthesis was carried out in a microwave reactor Monowave 400 (Anton Paar). Scanning electron microscopy (SEM) micrographies were acquired in a Supra-35 ZEISS FESEM system and high resolution transmission electron microscopy (HR-TEM) images were obtained with a Tecnai G2, FEI microscope. X-ray diffraction patterns were obtained from a Shimadzu diffractometer model XRD-6000, electrode voltage 30 kV, Cu Kα radiation, in θ–2θ mode, at 1° s^{-1}. Electrochemical measurements were performed in an Autolab PGSTAT302 potentiostat (Eco Chemie), using a typical three-compartment electrochemical glass cell. The working electrode was a porous graphite substrate modified with the corresponding particles (MnO_2, bimetallic NPs or bimetallic NPs enclosed in MnO_2) and the counter electrode was a platinum wire. All potentials are reported versus the reversible hydrogen electrode (RHE). Raman spectra were acquired in a Renishaw *inVia* Raman microscope using a 20 mW HeNe laser (λ = 633 nm).

2.2. Synthesis of MnO_2 and $PtAu_3@MnO_2$

The synthesis of MnO_2 was carried out in a three-phase mixture consisting of toluene and 2 M aqueous solution of $MnSO_4$, containing solid $(NH_4)_2S_2O_8$ as the oxidant agent (20:1, molar ratio). The solid oxidant agent was mixed with the organic phase in a MW glass reactor and the $MnSO_4$ was added afterwards. The reactor

was inserted in the MW reaction chamber and the reaction was performed at 180 °C for 20 min. Upon completion of the reaction, the organic phase was discarded and the MnO_2 particles in the aqueous phase were centrifuged and washed with water several times and dried at 60 °C overnight. In the case of the synthesis of $PtAu_3@MnO_2$ composites, 0.5 mg of PtAu bimetallic nanoparticles (1:3 molar ratio, $PtAu_3$) dispersed in water were mixed with the solution containing $MnSO_4$ and the reaction was carried out under the same conditions. Working electrodes were prepared by dropping a dispersion of ethanol containing 2 mg of the as-prepared particles on graphite substrates and drying them at 100 °C.

3. Results and discussion

3.1. Structural and morphological characterization

Fig. 1 shows the SEM images at different magnifications of the as-synthesized MnO_2 particles. Particles are ca. 1.5 μm diameter and show dandelion-like structure with hollow core. We assume that this singular structure is a consequence of the microwave dielectric heating and of the introduction of an organic phase in the reaction media, which allows slow interaction of the manganese precursor and the oxidant agent. In addition to the slow mass transport, the electromagnetic field will couple more strongly with water than with toluene (loss factor 0.123 and 0.040 at 2.45 GHz, respectively) [22], generating different temperature distributions and, therefore, selectively heating the MnO_2 solution [19]. The third solid phase is suggested to play an important role in the reaction mechanism, attributed to the high coupling of microwaves with solids, which generally generates hot spots. The generation of hot spots has been previously reported to promote local higher temperatures compared to the bulk, of the order of 100–200 K, provoking shifts in the equilibrium constant [30–32].

In order to show the capability of these structures as containers for nanomaterials, $PtAu_3$ bimetallic catalysts have been caged inside the MnO_2 cavity. We used $PtAu_3$ NPs as a reference material, previously well characterized and which has been proved to show good catalytic properties toward the oxidation of formic acid [33]. The synthesis of $PtAu@MnO_2$ composites was carried out under the same conditions of the synthesis described for MnO_2, but adding the previously synthesized $PtAu_3$ NPs to the solution containing $MnSO_4$. Under these synthesis conditions, it can be observed in the SEM images (Fig. 2) that, after PtAu NPs inclusion, MnO_2 particles show less open structure, probably as a consequence of growing around the nanoparticles, showing a star-like configuration (Fig. 2A), which seems not to have a solid core. SEM image using BSE detector (Fig. 2B) show that the PtAu particles are embedded inside the MnO_2 and Fig. 2C and D show the HR-TEM images of the MnO_2 needles from Fig. 2A. It can be clearly observed that there is not a solid core, which may allow species diffusion inside the MnO_2 structure. Outer needles are ca. 45 nm thick with a well-defined growth plane.

The bulk composition of the $PtAu@MnO_2$ composites was estimated by Energy-Dispersive X-ray Spectroscopy (EDS). EDX spectrum performed on isolated MnO_2 particles (Fig. 3A) confirms that the structures contain Au and Pt, in addition to Mn. (physical characterization of PtAu nanoparticles, by XPS and XRD, demonstrating Pt and Au content has been previously reported) [33].

Absorbance profiles of colloidal gold nanoparticles (synthesized under the same conditions that PtAu nanoparticles, but in the absence of the platinum precursor) and of $PtAu_3$ nanoparticles are represented in Fig. 3B, for comparison. Au NPs show the characteristic surface plasmon band with maximum absorbance at 526 nm, which may be related to particles with ca. 30 nm diameter [34,35]. On the other hand, PtAu bimetallic nanoparticles showed
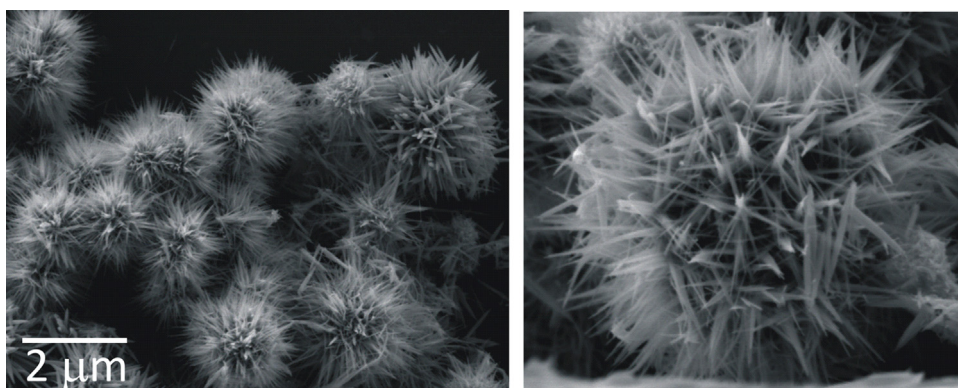
Fig. 1. SEM micrographies of hollow MnO_2 particles synthesized by microwave-assisted hydrothermal route.
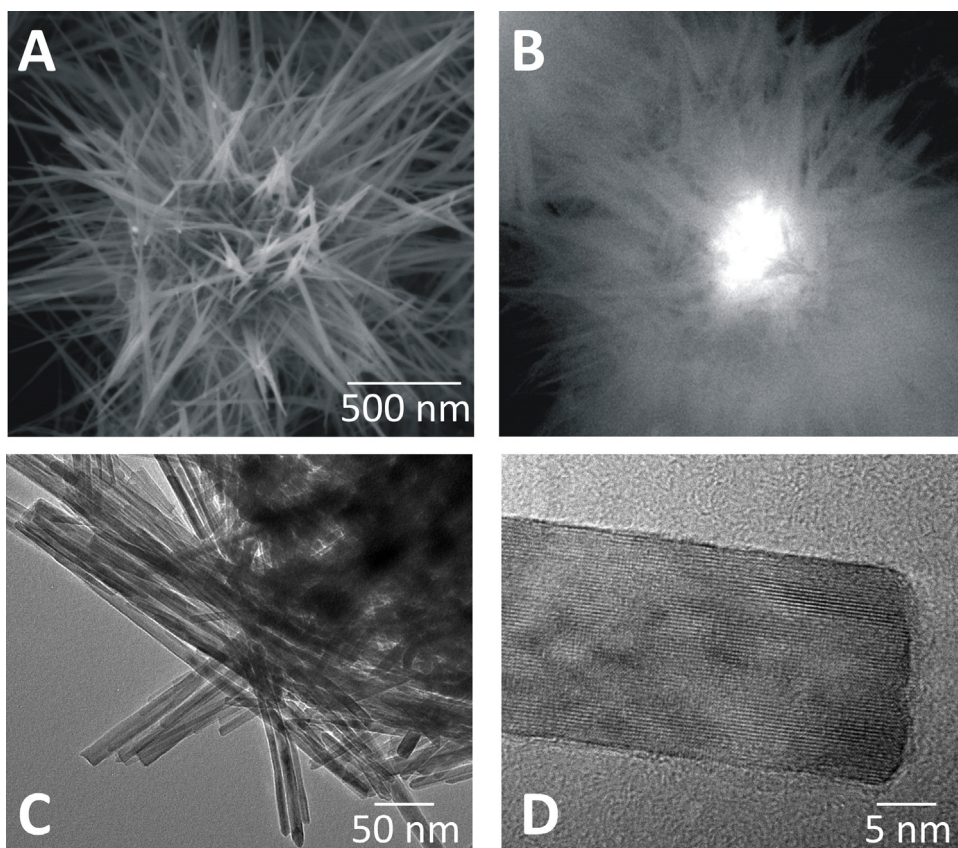
Fig. 2. SEM micrographies of (A) PtAu@MnO_2 composites synthesized by microwave-assisted hydrothermal route and (B) $PtAu_3$ enclosed in MnO_2 particles (using BSE detector); (C and D) HR-TEM images of the MnO_2 outer needles.

no plasmon absorbance bands. In general, gold nanocomposites are expected to exhibit different surface plasmon resonance properties compared to bare gold [36]. In our case, the absence of absorbance band supported the formation of an alloy, in good agreement with previous findings where it was demonstrated that the presence of metals from Group 10 in bimetallic nanoparticles, lead to the suppression of SPR energies of Group 11 metals [37,38].

Fig. 3C shows the XRD patterns of the MnO_2, PtAu3 and PtAu@MnO_2 composites. MnO_2 diffraction peaks at 2θ: 12.8°, 18.2°, 28.8°, 37.5°, 41.1°, 42.9°, 49.9°, 56.8°, 65.2°, 69.3°, 72.7° can be indexed according to JCPDS #44-141 and corresponds to the tetragonal crystalline phase structure concordant with the allotropic form α-MnO_2. XRD patterns of the as-synthesized $PtAu_3$ NPs have been previously reported [33]. Briefly, bimetallic PtAu particles show face centered cubic (*fcc*) structure, with high crystallinity.

All peaks corresponding to both, Au (JCPDS #4784) and Pt (JCPDS #4802) can be observed, confirming the presence of both elements. The difractogram profile obtained for the PtAu@MnO_2 composites is a combination of those obtained for MnO_2 and $PtAu_3$ particles in which all peaks of MnO_2, Pt and Au are present. These results corroborate those obtained by SEM, demonstrating the presence of PtAu particles inside the MnO_2 cages and that the inclusion of PtAu particles in the synthesis process of MnO_2 does not affect their structural properties (Fig. 2A and B).

Raman spectroscopy is suitable to characterize manganese oxides, despite of the low Raman cross section of manganese oxide [39]. Both samples, MnO_2 and PtAu@MnO_2 (Fig. 4), showed a broad band centered at $634\,cm^{-1}$, characteristic of to the ν_{sym}(Mn-O) of the MnO_6 group double chains typical of 2x2 tunnels of α-MnO_2 [40], which is in good agreement with the results obtained by
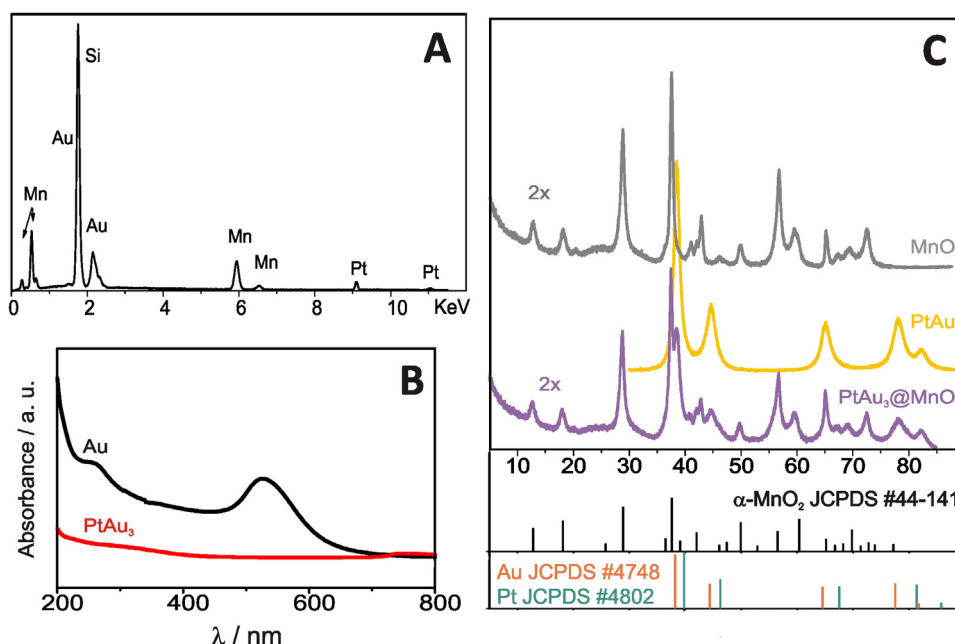
Fig. 3. (A) EDX spectrum of PtAu@MnO$_2$ composites; (B) UV/vis spectra on Au and PtAu$_3$ nanoparticles; (C) XRD patterns of MnO$_2$; PtAu$_3$ (yellow) and PtAu@MnO$_2$ particles, corresponding to JCPDS #44-141 (α-MnO$_2$), #4-748 (Au) and #4-802 (Pt).
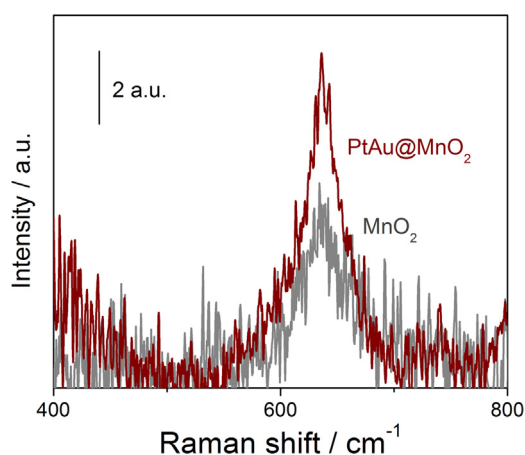
Fig. 4. Raman spectra of MnO$_2$ particles and PtAu@MnO$_2$ composites.

XRD. Other characteristic bands ascribed to α-MnO$_2$, δ(Mn-O) and ν_{sym}(Mn-O) in basal plane of the MnO$_6$ sheet, were not observed probably due to the low energy excitation laser. Raman spectra for MnO$_2$ samples are usually acquired under 514 nm laser excitation and long accumulation times, because of the low Raman activity. However, under these experimental conditions, it may be possible to induce photo or thermal chemical reactions misleading shifts and broadening of the Raman modes [39]. For this reason, we have used a 633 nm laser, preferring the loss of intensity to the degradation of the sample. Independently, Raman experiments demonstrate that the introduction of PtAu Nps in the synthesis route of MnO$_2$ do not affect its structural properties, suggesting a wide possibility of species to be enclosed inside the MnO$_2$ cavity.

3.2. Applications

Due to the low stability of MnO$_2$ in acidic media, the potential applications of these structures may be limited to neutral and/or alkaline media. In such a way, and just as possible examples of applications, we have used them as cathodes for the reduction of oxygen and as anodes for the oxidation of glycerol. In both cases, the working electrode was a high-surface area graphite electrode (blank) and graphite electrodes containing 2 mg of particles. Three electrodes were prepared, containing MnO$_2$, PtAu$_3$ NPs and PtAu@MnO$_2$ composites. All experiments were performed in 1 M KOH.

3.2.1. Glycerol electrooxidation

In recent years, the search for an industrial application for glycerol has become a topic of interest in research. Glycerol (Gly) is a byproduct of the biofuel industry. Therefore, an effective use of glycerol may be considered essential for biodiesel suitability. In such a way, several different applications for the practical utilization of crude glycerol have been proposed, including feedstock for chemicals [41,42]; production of hydrogen [43,44], etc. Among them, the use of glycerol as fuel for direct alcohol fuel cells (DAFCs) [45–48] should be highlighted in addition to the search of novel anode electrocatalysts to replace platinum or to decrease the amount of Pt.

Electroactivity of the hollow MnO$_2$ particles loaded with PtAu nanoparticles toward the glycerol oxidation in alkaline media is shown in Fig. 5A (normalized to the mass of PtAu$_3$ nanoparticles, when corresponding). Bare graphite (i) and MnO$_2$ (ii) electrodes do not show any activity toward this reaction, in contrast to those loaded with PtAu nanoparticles (iii and iv). PtAu$_3$ nanoparticles show activity toward the oxidation of glycerol as demonstrated by the two anodic peaks found in the forward scan (iii). The electrooxidation of glycerol has been previously reported on Pt-Au bimetallic catalysts [49] and it has been shown to follow complex reaction pathways [50]. The oxidation of glycerol during the positive-going sweep begins at 0.42 V (potential at which the oxidation current exceeds by 5% the baseline current) giving a well-defined Peak I at 0.93 V and a second smaller Peak II at 1.32 V. After Peak II, the current rapidly decreases because of the formation of surface oxides on the NPs surface and consequently reduction of catalytic active sites. This oxide layer is reduced during the anodic backwards scan, providing free catalytic sites and the glycerol electrooxidation takes place again (Peaks III and IV, 1.17 V and 0.72 V, respectively). In general, voltammetric peaks obtained in the oxidation of glycerol
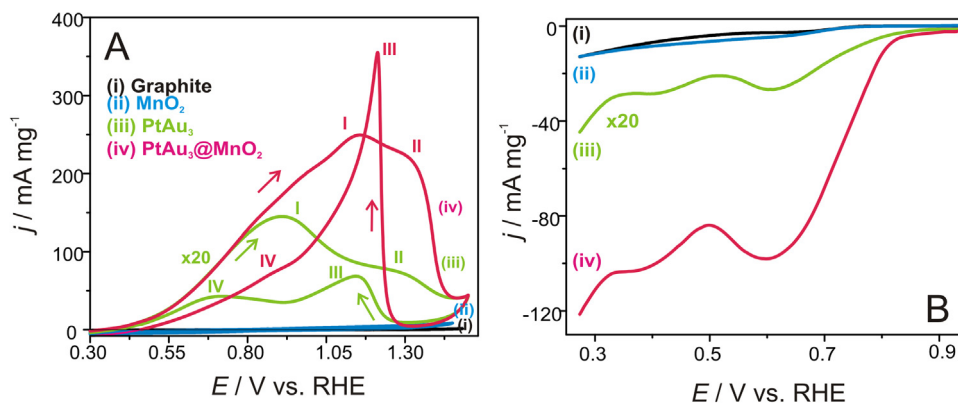
Fig. 5. (A) LSV measurements of bare graphite electrode (i); and graphite electrode loaded with MnO_2 particles (ii); $PtAu_3$ nanoparticles (iii) and $PtAu@MnO_2$ composites (iv) in a solution containing 1 M KOH, O_2 saturated at a scan rate of 0.05 V s^{-1}. (B) Cyclic voltammograms of bare graphite electrode (i); and graphite electrode loaded with MnO_2 particles (ii); $PtAu_3$ nanoparticles (iii) and $PtAu@MnO_2$ composites (iv) in a solution containing 0.1 M glycerol and 1 M KOH, N_2 saturated, at a scan rate of 0.05 V s^{-1}.

are broad, since they are active over a wide potential window. In the case of $PtAu@MnO_2$ electrodes (iv) the cyclic voltammetry profiles show that the oxidation of glycerol is occurring, demonstrating that there is mass transport throughout the MnO_2 shell. In the anodic forward scan, a broad shoulder can be observed from 0.78 V to 1.08 V before Peak I at 1.2 V. Peak II appears at 1.35 V and currents drops at higher potentials because of the oxide formation. The anodic backwards sweep shows a high current sharp Peak III at 1.25 V and Peak IV is shown as a low intensity shoulder at 0.90 V, which may be related to a reduced rate of glycerol adsorption on the reduced PtAu surface during the backwards potential sweep [50].

In this case, the reaction begins ca. 100 mV more positive that in the case of the $PtAu_3$ electrode, which may be explained in terms of mass transport limitation, attributed to diffusional resistances across the MnO_2 network and this affecting the reaction kinetics. On the other hand, currents achieved with $PtAu@MnO_2$ electrodes are much higher than those obtained with $PtAu_3$ electrodes (up to 40 times) and considering that the catalyst mass is ca. 10 times smaller. The reaction mechanism may be explained in terms of changes in current with Gly and hydroxide concentration and reaction kinetics ascribed to adsorption of Gly intermediates and hydroxyl. This suggests that mass transport limitations, in this case, are preventing diffusion of intermediate reaction species to the bulk electrolyte and leading to a higher overall reaction efficiency.

3.2.2. ORR

The reduction of the cathode overpotential for the oxygen reduction reaction is still a remaining topic of interest in research, concerning the development and commercial applications of low temperature fuel cells and metal–air batteries. In such a way, the search of cost-effective materials with improved efficiency toward the ORR, which in addition may conduct the reaction via the direct 4-electron reduction pathway from O_2 to H_2O [51] are highly desirable. However, most of catalysts conduct the reaction throughout a sequence of steps which evolves H_2O_2 as intermediate leading to losses in cell potential further reduced by consequent reduction of the formed peroxide [51].

$$O_{2(ads)} + e^- \rightarrow O_{2(ads)}^- \tag{1}$$

$$O_{2(ads)}^- + H_2O + 2e^- \rightarrow HO_{2(ads)}^- + OH^- \tag{2}$$

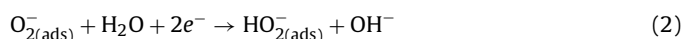$$HO_2^- + H_2O + 2e^- \rightarrow 3OH^- \tag{3}$$

Fig. 5B shows the linear sweep voltammetric profiles obtained for the ORR for all the electrodes, and normalized to the mass of $PtAu_3$ nanoparticles, when corresponding. Bare graphite (i) and

MnO_2 electrodes (ii) show low electrocatalytic activity toward the ORR compared to PtAu and $PtAu@MnO_2$ electrodes (iii and iv, respectively), as shown by the LSV profiles. In the case of the $PtAu_3$ electrodes (iii), two cathodic irreversible peaks can be clearly observed, which have been previously ascribed to the ORR following two consecutive reaction steps [52]. Peak I at 0.59 V describes the electroreduction of oxygen into hydrogen peroxide via 2 electrons (Eqs. (1) and (2)) and Peak II at 0.19 V is the subsequent reduction to water (Eq. (3)). Profiles obtained from $PtAu@MnO_2$ electrodes (iv) are similar to those obtained with $PtAu_3$ electrodes but, again, showing much higher current densities. In this case, the manganese oxide network do not represent a limitation for the diffusion of oxygen to the catalyst surface, but seems to limit diffusion of reaction intermediates to the bulk electrolyte, leading to enhanced electrocatalytic efficiency.

MnO_2 catalytic activity has been prove to be strongly dependent on the crystallographic phase, following an order α-> β-> γ-MnO_2 [53] attributed to 2 × 2 tunnels of α-MnO_2. In such a way, α-MnO_2 nanostructures have been proved to show good electrocatalytic performance toward the ORR in alkaline media. It should be pointed up that our MnO_2 structures show higher catalytic activity toward the ORR in alkaline media (up to ca. three-fold) compared to others reported in literature [53–55] even under the claim that these materials show lower electrocatalytic performance compared to PtAu nanoparticles and PtAu nanoparticles enclosed in the hollow cavity of the MnO_2 frameworks. Further, noble metal nanoparticles with a MnO_2 shell have been successfully applied for the ORR in alkaline media, such as Pd [56,57], Au [57,58] and Pt [55,59,60] with results (comparing current densities) much lower than those obtained with our material. In a lower extent, MnO_2 based architectures have been also used for the oxidation of glycerol [61], showing again lower efficiencies compared to our results, and this confirming the good catalytic performance of our metal-loaded inorganic frameworks. These results suggest a great opportunity for the development of new catalysts with potential applications in different research fields.

3.3. Stability tests

The long-term performance the electrodes containing PtAu particles was investigated for the electrooxidation of glycerol by chronoamperometry, under an applied potential corresponding to the maximum current density of the voltammetric anodic peak (Fig. 6). Current densities in 0.1 M glycerol and 1 M KOH remained essentially constant after 60 h polarization with no evidences of loss of activity, proving their high stability and the ability of the MnO_2 cages to keep the nanoparticle in their inner cavity.
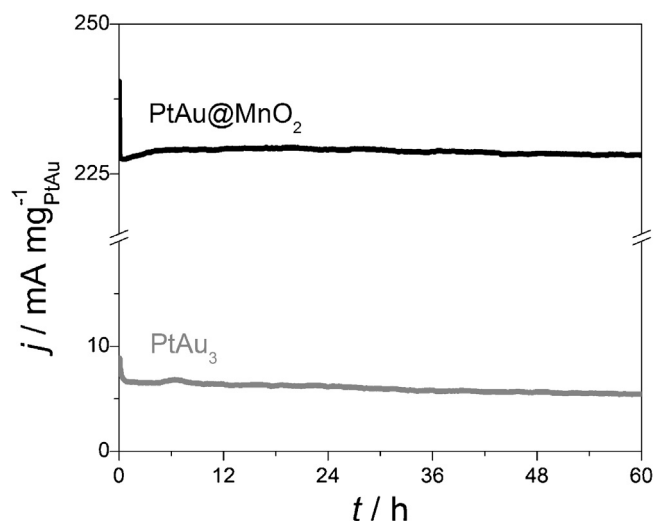
Fig. 6. Chronoamperometric profiles for PtAu$_3$ (grey line) and PtAu@MnO$_2$ (black line) electrodes, performed in a solution containing 0.1 M glycerol and 1 M KOH under an applied potential corresponding to the maximum current density of the voltammetric anodic peak (Fig. 5A).

4. Conclusion

We have developed an easy, fast method of synthesis of hollow MnO$_2$ particles via microwave-assisted hydrothermal route. In addition, we have demonstrated the ability of these structures to enclose smaller species, such as PtAu bimetallic nanoparticles without the need of a template. PtAu@MnO$_2$ composites showed to have enhanced electrocatalytic activity toward the oxidation of glycerol and the oxygen reduction reaction in alkaline media, compared to bare PtAu particles, what we attribute to the MnO$_2$ cage, which is responsible for the confinement of reaction intermediates impeding their diffusion to the bulk electrolyte.

Considering the inherent properties of MnO$_2$, such as low acute toxicity to living organisms, biocompatibility, stability in neutral and alkaline media and the ability to enclose other different materials, including functionalized nanoparticles, we suggest a broad field of potential application for these structures, such as drug delivery and bioimaging, catalysis, (bio)sensing, etc.

Acknowledgements

References

[1] X. Luo, A. Morrin, A.J. Killard, M.R. Smyth, Application of nanoparticles in electrochemical sensors and biosensors, Electroanalysis 18 (2006) 319–326.

[2] K. Song, J. Jung, Y.-U. Heo, Y.C. Lee, K. Cho, Y.-M. Kang, [small alpha]-MnO2 nanowire catalysts with ultra-high capacity and extremely low overpotential in lithium-air batteries through tailored surface arrangement, Phys. Chem. Chem. Phys. 15 (2013) 20075–20079.

[3] M. Fekete, R.K. Hocking, S.L.Y. Chang, C. Italiano, A.F. Patti, F. Arena, L. Spiccia, Highly active screen-printed electrocatalysts for water oxidation based on [small beta]-manganese oxide, Energy Environ. Sci. 6 (2013) 2222–2232.

[4] R.B. Valim, M.C. Santos, M.R.V. Lanza, S.A.S. Machado, F.H.B. Lima, M.L. Calegaro, Oxygen reduction reaction catalyzed by ε-MnO2: Influence of the crystalline structure on the reaction mechanism, Electrochim. Acta 85 (2012) 423–431.

[5] B.B. Lakshmi, C.J. Patrissi, C.R. Martin, Sol-Gel template synthesis of semiconductor oxide micro- and nanostructures, Chem. Mater. 9 (1997) 2544–2550.

[6] V. Subramanian, H. Zhu, B. Wei, Synthesis and electrochemical characterizations of amorphous manganese oxide and single walled carbon nanotube composites as supercapacitor electrode materials, Electrochem. Commun. 8 (2006) 827–832.

[7] I. Zaharieva, P. Chernev, M. Risch, K. Klingan, M. Kohlhoff, A. Fischer, H. Dau, Electrosynthesis, functional, and structural characterization of a water-oxidizing manganese oxide, Energy Environ. Sci. 5 (2012) 7081–7089.

[8] R.N. Reddy, R.G. Reddy, Sol-gel MnO2 as an electrode material for electrochemical capacitors, J. Power Sources 124 (2003) 330–337.

[9] R.N. Reddy, R.G. Reddy, Synthesis and electrochemical characterization of amorphous MnO2 electrochemical capacitor electrode material, J. Power Sources 132 (2004) 315–320.

[10] B. Gnana Sundara Raj, A.M. Asiri, A.H. Qusti, J.J. Wu, S. Anandan, Sonochemically synthesized MnO2 nanoparticles as electrode material for supercapacitors, Ultrason. Sonochem. 21 (2014) 1933–1938.

[11] M. Ghaemi, F. Ataherian, A. Zolfaghari, S.M. Jafari, Charge storage mechanism of sonochemically prepared MnO2 as supercapacitor electrode: effects of physisorbed water and proton conduction, Electrochim. Acta 53 (2008) 4607–4614.

[12] V. Subramanian, H. Zhu, R. Vajtai, P.M. Ajayan, B. Wei, Hydrothermal synthesis and pseudocapacitance properties of MnO2 nanostructures, J. Phys. Chem. B 109 (2005) 20207–20214.

[13] A. Bello, O.O. Fashedemi, M. Fabiane, J.N. Lekitima, K.I. Ozoemena, N. Manyala, Microwave assisted synthesis of MnO2 on nickel foam-graphene for electrochemical capacitor, Electrochim. Acta 18 (2013) 48–53.

[14] L.R. Pahalagedara, S. Dharmarathna, C.K. King'ondu, M.N. Pahalagedara, Y.T. Meng, C.H. Kuo, S.L. Suib, Microwave-Assisted hydrothermal synthesis of α-MnO2: lattice expansion via rapid temperature ramping and framework substitution, J. Phys. Chem. C 118 (2014) 20363–20373.

[17] A. Stadler, B.H. Yousefi, D. Dallinger, P. Walla, E. Van der Eycken, N. Kaval, C.O. Kappe, Scalability of microwave-assisted organic synthesis. from single-mode to multimode parallel batch reactors, Org. Process Res. Dev. 7 (2003) 707–716.

[18] P. Lidström, J. Tierney, B. Wathey, J. Westman, Microwave assisted organic synthesis—a review, Tetrahedron 57 (2001) 9225–9283.

[19] S. Horikoshi, N. Serpone, Role of microwaves in heterogeneous catalytic systems, Catal. Sci. Technol. 4 (2014) 1197–1210.

[20] A. Ferrari, J. Hunt, A. Stiegman, G. Dudley, Microwave-assisted superheating and/or microwave-specific superboiling (Nucleation-Limited Boiling) of liquids occurs under certain conditions but is mitigated by stirring, Molecules 20 (2015) 19793.

[21] C. Gabriel, S. Gabriel, E.H. Grant, B.S.J. Halstead, D. Michael, P. Mingos, Dielectric parameters relevant to microwave dielectric heating, Chem. Soc. Rev. 27 (1998) 213–224.

[22] T. Maugard, D. Gaunt, M.D. Legoy, T. Besson, Microwave-assisted synthesis of galacto-oligosaccharides from lactose with immobilized β-galactosidase from Kluyveromyces lactis, Biotechnol. Lett. 25 (2003) 623–629.

[23] M.B. Gawande, S.N. Shelke, R. Zboril, R.S. Varma, Microwave-assisted chemistry synthetic applications for rapid assembly of nanomaterials and organics, Acc. Chem. Res. 47 (2014) 1338–1348.

[24] K.J. Major, C. De, S.O. Obare, Recent advances in the synthesis of plasmonic bimetallic nanoparticles, Plasmonics 4 (2009) 61–78.

[25] K. Richter, P.S. Campbell, T. Baecker, A. Schimitzek, D. Yaprak, A.-V. Mudring, Ionic liquids for the synthesis of metal nanoparticles, Phys. Status Solidi (b) 250 (2013) 1152–1164.

[26] N. Chopra, L. Claypoole, L.G. Bachas, Morphological control of Ni/NiO core/shell nanoparticles and production of hollow NiO nanostructures, J. Nanopart. Res. 12 (2010) 2883–2893.

[27] R. Purbia, S. Paria, Yolk/shell nanoparticles: classifications, synthesis, properties, and applications, Nanoscale 7 (2015) 19789–19873.

[28] L. Wang, Y. Yamauchi, Metallic nanocages synthesis of bimetallic Pt-Pd hollow nanoparticles with dendritic shells by selective chemical etching, JACS 135 (2013) 16762–16765.

[29] R. Singh, J.W. Lillard Jr., Nanoparticle-based targeted drug delivery, Exp. Mol. Pathol. 86 (2009) 215–223.

[30] X. Zhang, D.O. Hayward, D. Michael, P. Mingos, Apparent equilibrium shifts and hot-spot formation for catalytic reactions induced by microwave dielectric heating, Chem. Commun. (1999) 975–976.

[31] Y. Tsukahara, A. Higashi, T. Yamauchi, T. Nakamura, M. Yasuda, A. Baba, Y. Wada, In situ observation of nonequilibrium local heating as an origin of special effect of microwave on chemistry, J. Phys. Chem. C 114 (2010) 8965–8970.

[32] S. Horikoshi, A. Osawa, S. Sakamoto, N. Serpone, Control of microwave-generated hot spots. Part V. Mechanisms of hot-spot generation and aggregation of catalyst in a microwave-assisted reaction in toluene catalyzed by Pd-loaded AC particulates, Appl. Catal. A 460–461 (2013) 52–60.

[33] G. Cabello, R.A. Davoglio, F.W. Hartl, J.F. Marco, E.C. Pereira, S.R. Biaggio, H. Varela, A. Cuesta, Microwave-assisted synthesis of Pt-Au nanoparticles with enhanced electrocatalytic activity for the oxidation of formic acid, Electrochim. Acta 224 (2017) 56–63.

[34] V. Amendola, M. Meneghetti, Size evaluation of gold nanoparticles by UV–vis spectroscopy, J. Phys. Chem. C 113 (2009) 4277–4285.

[35] S. Link, M.A. El-Sayed, Size and temperature dependence of the plasmon absorption of colloidal gold nanoparticles, J. Phys. Chem. B 103 (1999) 4212–4217.

[36] S. Moussa, V. Abdelsayed, M.S. El Shall, 1 − Chemical Synthesis of Metal Nanoparticles and Nanoalloys A2 − Calvo, Florent, Nanoalloys, Elsevier, Oxford, 2013, pp. 1–37.

[37] N. Toshima, T. Yonezawa, Bimetallic nanoparticles-novel materials for chemical and physical applications, New J. Chem. 22 (1998) 1179–1201.

[38] L. Usón, V. Sebastian, A. Mayoral, J.L. Hueso, A. Eguizabal, M. Arruebo, J. Santamaria, Spontaneous formation of Au-Pt alloyed nanoparticles using pure nano-counterparts as starters: a ligand and size dependent process †Electronic supplementary information (ESI) available: supplementary STEM and EDS data. See Click here for additional data file, Nanoscale 7 (2015) 10152–10161, http://dx.doi.org/10.1039/c5nr01819f.

[39] R. Baddour-Hadjean, J.-P. Pereira-Ramos, Raman microspectrometry applied to the study of electrode materials for lithium batteries, Chem. Rev. 110 (2010) 1278–1319.

[40] Z.K. Ghouri, M. Shaheer Akhtar, A. Zahoor, N.A.M. Barakat, W. Han, M. Park, B. Pant, P.S. Saud, C.H. Lee, H.Y. Kim, High-efficiency super capacitors based on hetero-structured α-MnO2 nanorods, J. Alloys Compd. 642 (2015) 210–215.

[41] D.M. Alonso, S.G. Wettstein, J.A. Dumesic, Bimetallic catalysts for upgrading of biomass to fuels and chemicals, Chem. Soc. Rev. 41 (2012) 8075–8098.

[42] C.H. Christensen, J. Rass-Hansen, C.C. Marsden, E. Taarning, K. Egeblad, The renewable chemicals industry, ChemSusChem 1 (2008) 283–289.

[43] S. Adhikari, S.D. Fernando, A. Haryanto, Hydrogen production from glycerin by steam reforming over nickel catalysts, Renew. Energ. 33 (2008) 1097–1100.

[44] M. Slinn, K. Kendall, C. Mallon, J. Andrews, Steam reforming of biodiesel by-product to make renewable hydrogen, Bioresour. Technol. 99 (2008) 5851–5858.

[45] M. Simões, S. Baranton, C. Coutanceau, Electro-oxidation of glycerol at Pd based nano-catalysts for an application in alkaline fuel cells for chemicals and energy cogeneration, Appl. Catal. B 93 (2010) 354–362.

[46] K. Matsuoka, Y. Iriyama, T. Abe, M. Matsuoka, Z. Ogumi, Alkaline direct alcohol fuel cells using an anion exchange membrane, J. Power Sources 150 (2005) 27–31.

[47] V. Bambagioni, C. Bianchini, A. Marchionni, J. Filippi, F. Vizza, J. Teddy, P. Serp, M. Zhiani, Pd and Pt-Ru anode electrocatalysts supported on multi-walled carbon nanotubes and their use in passive and active direct alcohol fuel cells with an anion-exchange membrane (alcohol = methanol, ethanol, glycerol), J. Power Sources 190 (2009) 241–251.

[48] A. Zalineeva, A. Serov, M. Padilla, U. Martinez, K. Artyushkova, S. Baranton, C. Coutanceau, P.B. Atanassov, Self-Supported PdxBi catalysts for the electrooxidation of glycerol in alkaline media, JACS 136 (2014) 3937–3945.

[49] C.A. Ottoni, S.G. da Silva, R.F.B. De Souza, A.O. Neto, PtAu electrocatalyst for glycerol oxidation reaction using a ATR-FTIR/single direct alkaline glycerol/air cell In situ study, Electrocatalysis 7 (2016) 22–32.

[50] L. Roquet, E.M. Belgsir, J.M. Léger, C. Lamy, Kinetics and mechanisms of the electrocatalytic oxidation of glycerol as investigated by chromatographic analysis of the reaction products: potential and pH effects, Electrochim. Acta 39 (1994) 2387–2394.

[51] D.M. Dimarco, Oxygen Reduction on a Graphite Paste and a Catalyst Loaded Graphite Paste Electrode, AA(Ames Lab., IA.), Iowa State University, 1980, pp. 170.

[52] M.A. Ghanem, A.M. Al-Mayouf, M.N. Shaddad, F. Marken, Selective formation of hydrogen peroxide by oxygen reduction on TiO2 nanotubes in alkaline media, Electrochim. Acta 174 (2015) 557–562.

[53] Y. Meng, W. Song, H. Huang, Z. Ren, S.-Y. Chen, S.L. Suib, Structure-property relationship of bifunctional MnO2 nanostructures: highly efficient, ultra-stable electrochemical water oxidation and oxygen reduction reaction catalysts identified in alkaline media, JACS 136 (2014) 11452–11464.

[54] F. Cheng, Y. Su, J. Liang, Z. Tao, J. Chen, MnO2-based nanostructures as catalysts for electrochemical oxygen reduction in alkaline media, Chem. Mater. 22 (2010) 898–905.

[55] I. Roche, E. Chaînet, M. Chatenet, J. Vondrák, Carbon-supported manganese oxide nanoparticles as electrocatalysts for the oxygen reduction reaction (ORR) in alkaline medium: physical characterizations and ORR mechanism, J. Phys. Chem. C 111 (2007) 1434–1443.

[56] W. Sun, A. Hsu, R. Chen, Palladium-coated manganese dioxide catalysts for oxygen reduction reaction in alkaline media, J. Power Sources 196 (2011) 4491–4498.

[57] A.K. Thapa, T.H. Shin, S. Ida, G.U. Sumanasekera, M.K. Sunkara, T. Ishihara, Gold-Palladium nanoparticles supported by mesoporous β-MnO2 air electrode for rechargeable Li-air battery, J. Power Sources 220 (2012) 211–216.

[58] R. Imran Jafri, N. Sujatha, N. Rajalakshmi, S. Ramaprabhu, Au-MnO2/MWNT and Au-ZnO/MWNT as oxygen reduction reaction electrocatalyst for polymer electrolyte membrane fuel cell, Int. J. Hydrogen Energy 34 (2009) 6371–6376.

[59] P. Trogadas, V. Ramani, Pt/C/MnO2 hybrid electrocatalysts for degradation mitigation in polymer electrolyte fuel cells, J. Power Sources 174 (2007) 159–163.

[60] F.H.B. Lima, M.L. Calegaro, E.A. Ticianelli, Electrocatalytic activity of dispersed platinum and silver alloys and manganese oxides for the oxygen reduction in alkaline electrolyte, Russ. J. Electrochem. 42 (2006) 1283–1290.

[61] D. Padayachee, V. Golovko, A.T. Marshall, The effect of MnO2 loading on the glycerol electrooxidation activity of Au/MnO2/C catalysts, Electrochim. Acta 98 (2013) 208–217.